Chemical Engineering Journal 435 (2022) 135107

Contents lists available at ScienceDirect

Chemical Engineering Journal

journal homepage: www.elsevier.com/locate/cej

1 + 1 > 2: Dual strategies of quinolinic acid passivation and DMF solvent annealing for high-performance inverted perovskite solar cell

Yuheng Li [a,b,1], Dongyu Fan [a,b,1], Feiyang Xu [a,b], Chengwei Shan [b], Jiahao Yu [b], Wenhui Li [b], Dou Luo [b], Zonghao Sun [a], Hua Fan [a,b], Mengshuai Zhao [a], Xuehui Li [a], Kun Cui [a], Rui Chen [b], Gongqiang Li [a,c,*], Aung Ko Ko Kyaw [b,*]

[a] Key Laboratory of Flexible Electronic (KLOFE) & Institute of Advanced Materials (IAM), Nanjing Tech University (NanjingTech), 30 South Puzhu Road, Nanjing 211816, PR China
[b] Guangdong University Key Laboratory for Advanced Quantum Dot Displays and Lighting, and Department of Electrical & Electronic Engineering Southern University of Science and Technology Shenzhen 518055, PR China
[c] Wuhan National Laboratory for Optoelectronics (WNLO), Huazhong University of Science and Technology (HUST), Luoyu Road 1037, Wuhan 430074, Hubei, PR China

ARTICLE INFO

Keywords:
Inverted planar perovskite solar cell
Passivation
Solvent annealing
Dual strategies
Quinolinic acid

ABSTRACT

We developed a new combined method in which quinolinic acid (QA) passivation and DMF solvent annealing are carried out sequentially to enhance the performance of inverted perovskite solar cells. Upon systematic investigation, we found that: 1). One QA molecule not only passivates more than one defects within lattice or neighboring lattices, creating a multi-passivation effect, but also enhances the interactions between lattices, due to pyridine ring and dicarboxylic acid functional groups in the molecule; 2). By combining with DMF solvent annealing post-treatment sequentially, high quality perovskite films with very large grain size over 1 μm are obtained on the substrate of PEDOT: PSS. As a result, the PSC fabricated with the combined method demonstrates an excellent humidity stability and yields a PCE of 18.56% with 20% and 11.6% increment of V_{oc} and J_{sc}, respectively. To the best of our knowledge, it is the highest reported PCE for inverted PSCs with undoped PEDOT: PSS as hole transporting layer. Therefore, our work indicates that the combined strategy of multi-passivation with QA and solvent annealing with DMF sequentially has a significant potential for highly-efficient and stable inverted planar PSCs.

1. Introduction

Perovskite solar cells (PSCs) based on organic-inorganic lead halide perovskite (OIHP) [1-9] have attracted extensive attention during the last decade because of their great advantages such as: remarkable light absorption coefficient [10], adjustable energy level [11,12], long carrier diffusion length [13], very good defect tolerance [14] and solution-processed fabrication at room temperature [15,16]. The champion certified power conversion efficiency (PCE) of PSCs has been over 25% so far [17-19], which is comparable to that of silicon-based solar cells. However, non-radiative recombination mainly originating from the crystal defects, limits the performance of PSCs [20,21]. The defects in OIHP materials cause uncoordinated ions escaping from the perovskite structure [22], or grain boundaries and surface defects [23,24]. These defects create shallow level or deep level traps inside the bandgap depending on their formation energy. Although the trapped charges at the shallow levels can be re-emitted back to the band edges via phonon absorption, those at the deep levels cannot easily escape with the thermal activation and recombined with opposite carriers by non-radiative recombination as suggested by Shockley-Read-Hall theory. Nevertheless, the shallow defects still can accelerate the ion migration due to the ionic nature of OIHP materials and hence influence the device performance. Therefore, it is important to suppress defect states in perovskite solar cells to approach the radiative limit of efficiency and to guarantee the stability required under operational conditions.

The defect states in OIHP materials can be suppressed by the passivation with additives, which can be incorporated into perovskite films via adding them into precursor solutions [25], or anti-solvent [26],

* Corresponding authors.
E-mail addresses: iamgqli@njtech.edu.cn (G. Li), aung@sustech.edu.cn (A.K.K. Kyaw).
[1] They contributed equally to this work.

https://doi.org/10.1016/j.cej.2022.135107
Received 6 December 2021; Received in revised form 20 January 2022; Accepted 2 February 2022
Available online 5 February 2022

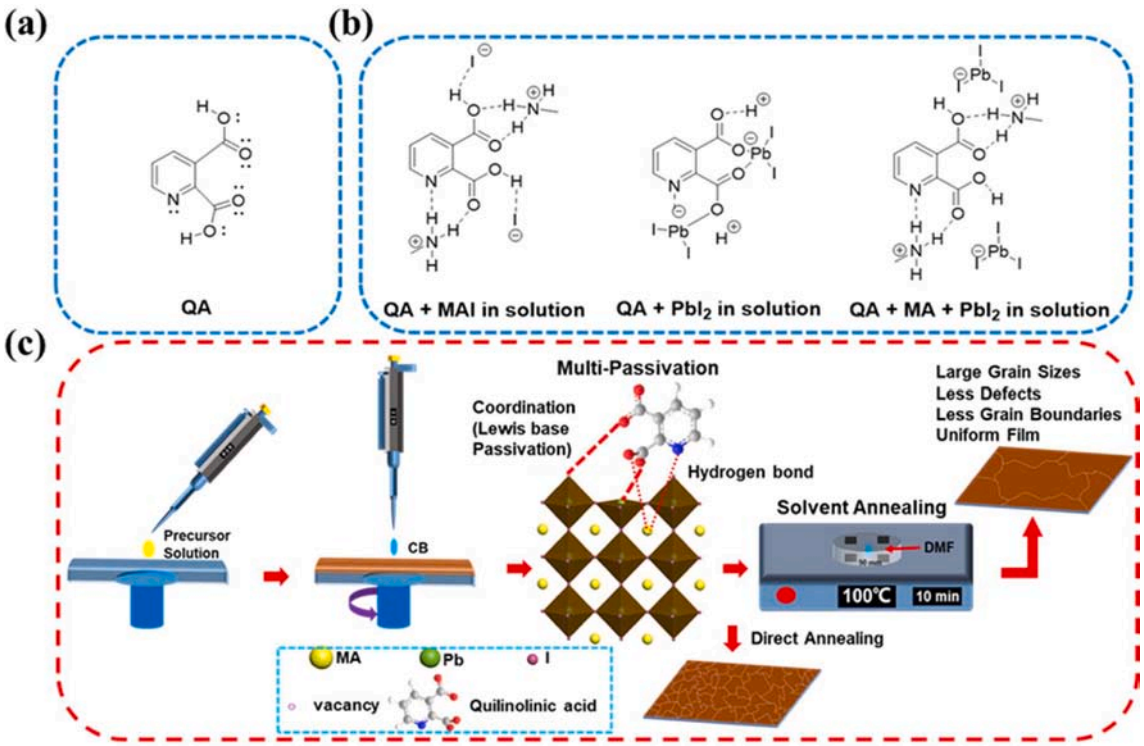

Fig. 1. (a) Chemical structure of quinolinic acid (QA). (b) Possible interactions between QA and perovskite precursors. (c) Fabrication chart of perovskite film with dual strategies and the passivation mechanism.

or post treatment [27]. Various additives such as Lewis acid, Lewis base, ammonium salts, ionic liquids, cations, anions, zwitterions etc. have been demonstrated to passivate different types of defects [25,28-32]. For instance, Lewis acid such as fullerene is effective to passivate the Pb–I antisite defects (PbI_3^-) and undercoordinated I^- ions, or to suppress ion migration at grain boundaries by accepting a lone pair of electrons [33,34]. In contrast, conjugated polymers or compounds with functional groups containing S, N, O donors act as Lewis base to passivate the undercoordination Pb^{2+} ions or metallic Pb cluster by donating a lone pair of electrons [35]. Cations and ammonium salts are suitable for passivation of negatively charged defects such as undercoordination I^-, Pb–I antisite, and cations (MA^+) vacancies via ionic or hydrogen bonding and electrostatic interactions with defects [36-38], while anions can be employed for positively charged defects such as undercoordination Pb^{2+} ions and I vacancies [39,40]. In the past few years, our group demonstrated the passivation of perovskite by employing various passivation agents including fluorinated conjugated polymer [41], organophosphorus ligand [42] and cyclooctatetrathiophene-based small molecule [43], which passivate the undercoordination Pb^{2+} defects by donating a lone pair electron from S, O atoms or formation of bonding. In addition to the passivation effect, some additives, for example sulfonate zwitterion demonstrated by Huang and co-workers, tune the crystallization behavior of perovskite, showing a dual role of additives [44].

The additives reported so far, however, usually contain only single active site for passivation, which means that one additive molecule can passivate only one defect site, and hence, they cannot efficiently passivate the multiple defect sites. Moreover, most of the additives are difficult to render the large grain size over 1 μm, but which is desirable because it can reduce grain boundaries and suppress the grain boundary defects. To overcome these limitations, firstly, we introduce quinolinic acid (QA) into precursors of methylammonium lead iodide ($MAPbI_3$) perovskite. As shown in Fig. 1, QA contains dicarboxylic acid (–COOH) group and one pyridine group, in which the O donor in carboxyl group can passivate defect sites associated with undercoordination Pb^{2+} ions, and trap MAI by forming hydrogen bonding to avoid it escaping the system during fabrication and annealing process, while N donor in pyridine group can passivate another defect site associated with I vacancies, or *vice versa*, via the lone pair electrons which facilitate the formation of a coordinate or dative covalent bond. All of these can effectively suppress the formation of vacancies and metallic Pb clusters. Hence, multi-passivation effects are induced by additive with bi-functional groups. As a result, the PCE of PSCs passivated with QA is higher than that of PSCs passivated with acetic acid or pyridine alone, especially in V_{oc}, due to the multi-passivation effects. Secondly, the passivated perovskite is further treated by solvent-annealing with dimethylformamide (DMF) to enlarge the grain sizes for obtaining high-quality perovskite films. As shown in Fig. 1c, the combined method of multi-passivation with QA and solvent-annealing with DMF leads to a high-quality films with very less pinhole but bigger grain sizes (over 1 μm), and a high PCE of 18.56% in inverted planar (p-i-n) PSCs with PEDOT:PSS as a hole transporting layer (HTL), which is higher than that of PSCs fabricated by passivation or solvent-annealing alone. In general, p-i-n PSCs with PEDOT:PSS HTL exhibits about 200 mV loss in V_{oc} compared to conventional n-i-p ones [45], but our champion device yields a very high V_{oc} of 1.07 V, which is close to the highest reported V_{oc} of p-i-n structure (~1.1 V) [46]. The high V_{oc} verifies that non-radiative recombination is effectively suppressed by multi-passivation effect and the large grain size. To the best of our knowledge, the PCE of 18.56% is the highest among the PSCs with undoped PEDOT:PSS, although a little higher PCE of 20.22% [45] and 19.66% [46] have been reported with doping PEDOT:PSS as summarized in Table S1. Additionally, the combined method of multi-passivation and solvent-annealing dramatically improves the stability of the device, and the devices fabricated by the combined method exhibit a much better humidity stability (90% of initial PCE is retained after keeping for more than 200 h in air with RH ~ 50% without any encapsulation) than that of the control device (90% of the initial value is retained after keeping only 25 h in the same condition). This synergistic combined method of multi-passivation and solvent-annealing opens a new way for improving the efficiency and

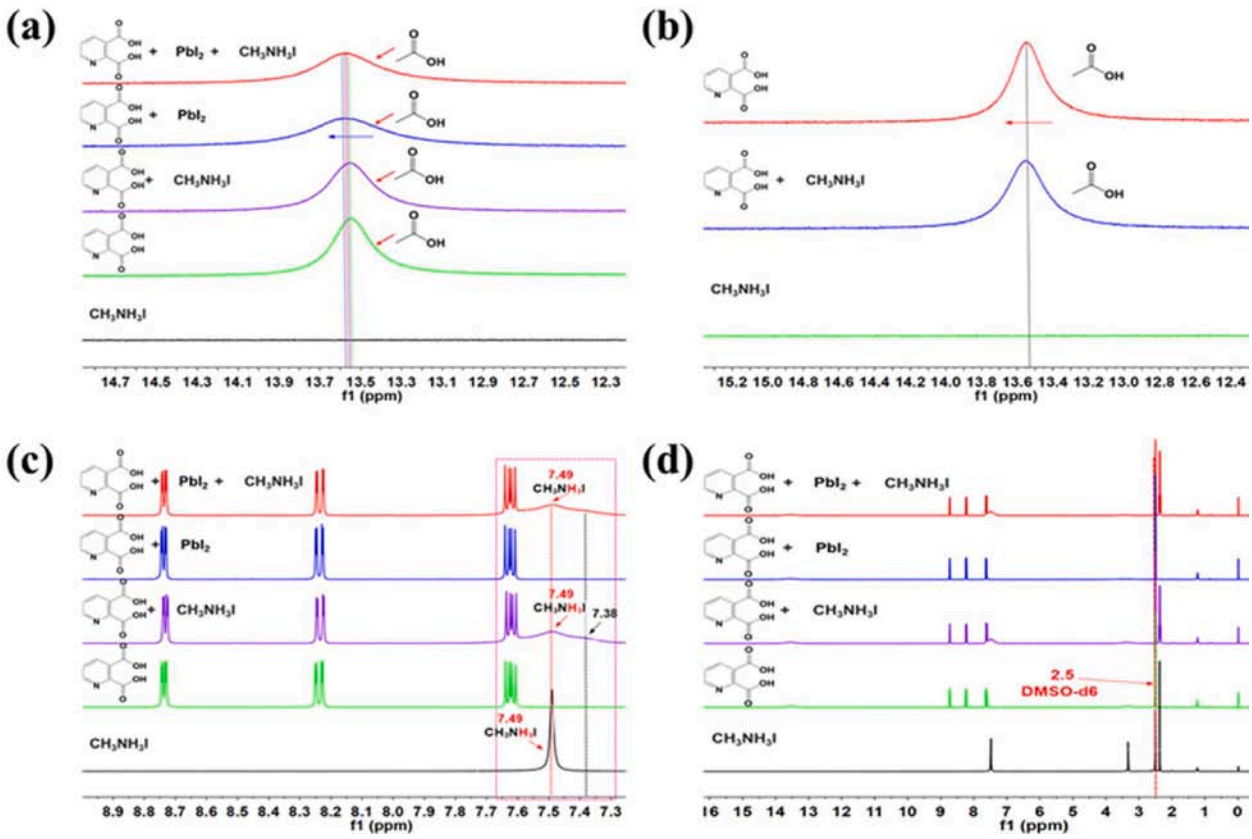

Fig. 2. ^{1}H NMR spectra of QA and perovskite precursors in DMSO-d_6: (a) Peak changes of carboxylic acid group. (b) Peak changes of MAI + QA. (c) Peak changes of H^+ of MA^+. (d) Full spectrum of QA and perovskite precursors.

stability of perovskite solar cells in the future.

2. Results and discussion

2.1. Interaction between QA and perovskite, and the passivation mechanism

The interaction between perovskite precursor and solvent is important to control over the dynamics of nucleation and grain growth of perovskite. It is recognized that the polar solvent such as DMF and dimethyl sulfoxide (DMSO) can interact with PbI_2 and form intermediate phase of MAI–PbI_2–solvent to seed nucleation [47]. However, the solvent escape is retarded due to the interaction between the perovskite precursors and high-boiling point solvent, so usually a high annealing process is required to obtain perovskite crystals. The high annealing temperature can cause damage to MAI, resulting in its absence in perovskite and producing more defects [48]. Additives of Lewis acids or bases, which are expected to strengthen the interaction with the perovskite precursor by acting as electron acceptors, donors or forming hydrogen bonding, can generate adducts of precursor-additive instead of precursor–solvent complexes [49]. Therefore, the perovskite crystals can be obtained at an appropriate temperature. Herein, phthalates derivative quinolinic acid (QA) is selected as additive, and the roles of carboxylic acid and pyridine ring groups is scrutinized.

Firstly, ^{1}H nuclear magnetic resonance (^{1}H NMR) spectroscopy was performed to investigate how the additive interacted with the perovskite precursor. As shown in Fig. 2, when QA is added into a solution of PbI_2, MAI, and PbI_2 + MAI in DMSO-d_6, respectively, just a very little shift of the peaks of –COOH at 13.55 ppm is observed, but the peaks become weaker and broader than that of original QA. The weakest and broadest peak at 13.55 ppm is observed in PbI_2 solution. The corresponding peak in PbI_2 + MAI solution is a little stronger than that in PbI_2, but it still weaker than that in MAI solution. All these demonstrated that the carboxylic acid groups have very strong interaction with PbI_2 by formation of Pb–O–coordination, while the interaction becomes weaker in PbI_2 + MAI, which may be caused by much more I vacancies in PbI_2 solution than in PbI_2 + MAI. Meanwhile, the sharp single peak of MA^+ at 7.49 ppm is drastically weakened into two broad peaks at 7.49 and 7.38 ppm in QA + MAI and QA + MAI + PbI_2 solutions (Fig. 2c), while the two peaks in QA + MAI solution seems no difference from these in QA + MAI + PbI_2. These indicate that MA^+ has very strong interaction with the carboxyl group and pyridine ring by forming a typical hydrogen bond. All in all, the interactions between QA and perovskite precursors by forming strong coordination with Pb^{2+} and forceful hydrogen bond with MA^+ in solution phase will suppress the formation of MA^+ or I^- vacancies and metallic Pb cluster, and also trap more MAI in the system to avoiding it escaping out during the fabrication and annealing process for balance reaction with PbI_2, all these advantages facilitate the formation of high-quality perovskite film with low trap density and large grain size [50].

Secondly, X-ray photoelectron spectroscopy (XPS) was conducted to further verify the change of core level binding energy of various elements in perovskite film after passivating with QA (Fig. S1, Supporting Information). Comparing with the control film, the passivated one reveals an existence of –C = O in the high resolution spectra of C 1s core level, indicating the successful incorporation of QA into the perovskite films and not escape (Fig. S1a, b, Supporting Information). Furthermore, the high resolution spectrum of N 1 s core level in passivated film displays an obvious shift (ca. 0.98 eV shift to low binding energy) compared to the control film due to the incorporation of QA (Fig. S2, Supporting Information). The spectra of I 3d and Pb 4f core level (Fig. S1c, d, Supporting Information) also reveal the shifts from low energy binding to high energy binding (0.25 eV and 0.15 eV, respectively) in the presence of QA, suggesting that defects associated with Pb^{2+} and I^- such as

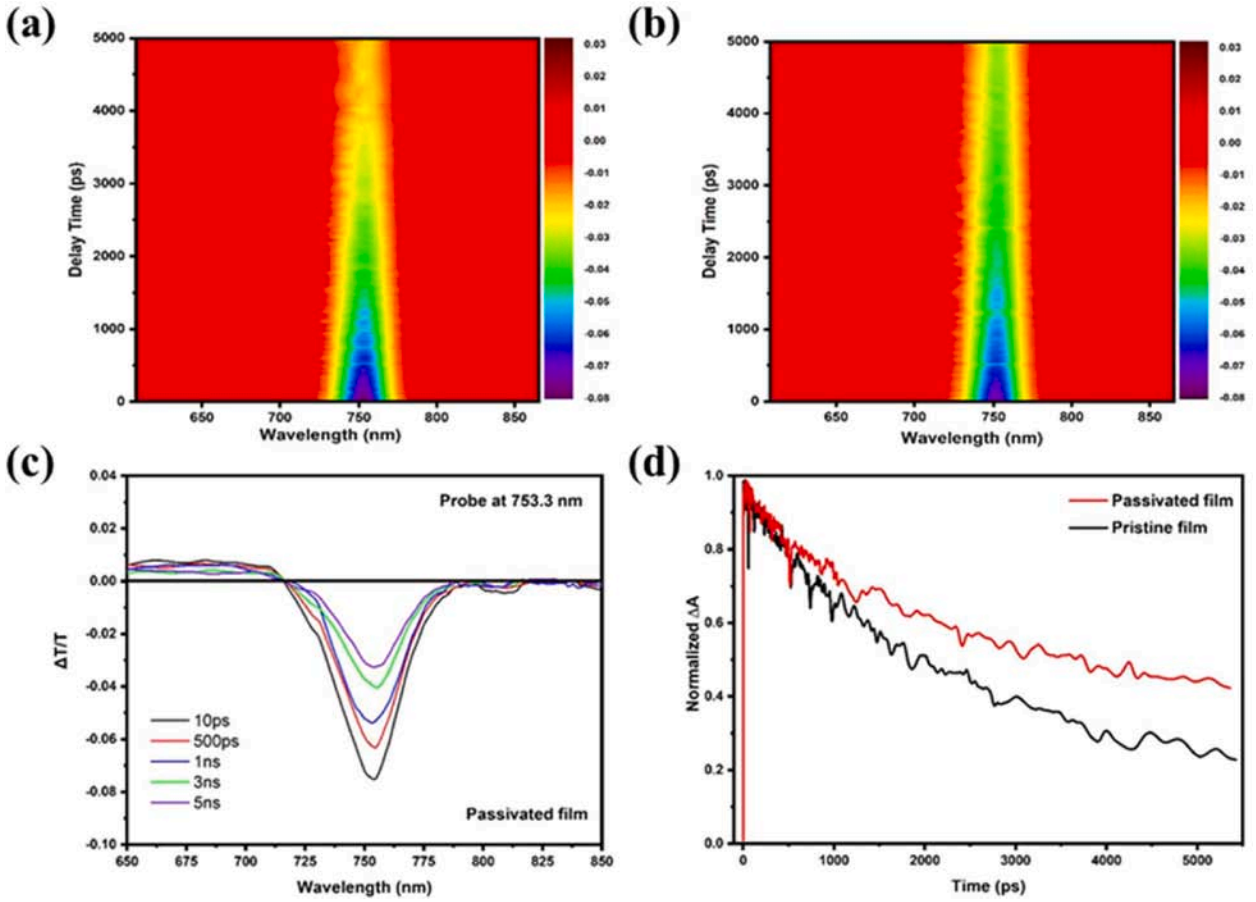

Fig. 3. Two-dimensional transient absorption spectra of perovskite films. (a) The control film. (b) The QA passivated film. (c) Deconvoluted species of TA spectra of the passivated film. (d) The dynamic lifetime curves of transient band edge bleaching of different films at 753 nm.

the incoordination Pb^{2+} ions and I^- vacancies are effectively passivated. It is worth noting that the peaks of metallic Pb_0 almost disappeared completely in the passivated film while they are very obvious in the control one. According to the lit. reported [51,52], the existence of metallic Pb_0 indicates the presence of iodide vacancies in the crystal lattice, which act as the non-radiative centers and also cause the instability of perovskite-based devices [53,54]. Hence, the QA may suppress the volatilization of component and retard the formation of metallic Pb_0 by a chemical interaction or passivate the defects originate from metallic Pb_0 clusters and I vacancies, all of which benefit for the formation of high-quality perovskite layer.

Based on the experimental data, we proposed the passivation mechanism of QA as following: In $MAPbI_3$ perovskite, various crystal imperfections such as undercoordination I^- ions, MA^+ vacancies, Pb-I antisites, undercoordination Pb^{2+} ions, I^- vacancies and metallic Pb_0 clusters can be populated on the surface and grain boundaries during crystallization process. Due to the nature of ions, undercoordination I^- ions, MA^+ vacancies and Pb-I antisites carry net negative charge while undercoordination Pb^{2+} ions, I^- vacancies and metallic cluster carry net positive charge. Owing to carrying net charge, these defect sites can easily capture the opposite photogenerated charge carriers and cause non-radiative recombination in the material. However, the net charge at the defect sites can be neutralized by creating a favorable condition for coordination or bond formation with electron-rich or electron-deficient molecules depending on the charge polarity of defect sites. Hence, the net negative charge carrying defect sites such as undercoordination I^- ions, MA^+ vacancies and Pb-I antisites can be passivated by coordination with electron acceptor (Lewis acid) while the net positive charge carrying defect sites such as incoordination Pb^{2+} ions, I^- vacancies and metallic Pb clusters can be passivated by electron donor (Lewis base).

QA is comprised of pyridine ring and dicarboxylic acid groups, the former can act as Lewis base, and latter not only can act as Lewis base by giving lone pair of electrons of O, but also can act as Lewis acid by giving H of C(O)OH to form hydrogen bonding (Fig. 1a, b). Hence, QA acts as Lewis base which is able to donate lone pair of electrons to defect sites with net positive charge such as undercoordination Pb^{2+} ions, I^- vacancies and metallic Pb clusters, which agree well with XPS result. The electrostatic attraction between the positive charge on the defect sites and lone pair of electrons from functional groups facilitates the formation of coordination or dative covalent bond, and hence, defect sites are neutralized and passivated. Since QA has three functional groups, one molecule can passivate several defect sites within lattice or neighboring lattices, creating the multi-passivation effect, which is different from other additives as reported before.

2.2. *Effect of passivation on carrier lifetime and photovoltaic properties*

Defect passivation of perovskite generally reduces trap density and increases carrier lifetime. So, the transient absorption spectroscopy (TAS) was carried out to study the dynamics of photogenerated carriers in perovskite films (Fig. 3a, b). Compared with the control film, the passivated one shows higher absorption for prolonged time, revealing a longer carrier lifetime due to defect passivation, which in turn reduces trap density. Meanwhile, from the two-dimensional spectrum, the peaks of ground state bleaching at 753 nm are derived and integrated into attenuation images of ground state bleaching (Fig. 3c, d). After a certain delay, the excitons are captured by the defects and the number of excitons remaining in the excited state decreases gradually. By fitting the

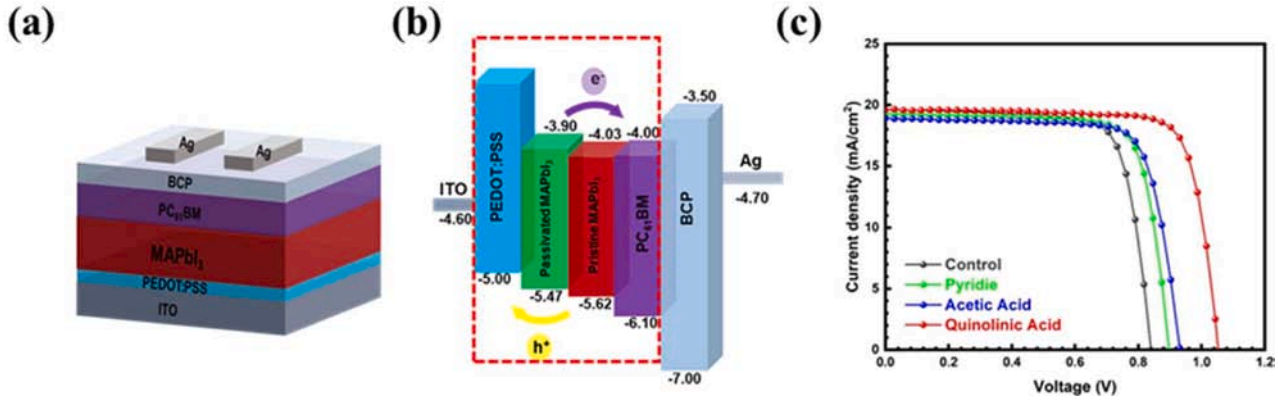

Fig. 4. (a) Device structure. (b) Energy levels of individual layers in the device. (c) Device performance with different additives.

attenuation curve of the ground state bleaching of the perovskite film, the τ_{avg} of the control film is 2.7 ns, while the τ_{avg} of the QA passivated one is 3.8 ns. The longer carrier lifetime suggests that the trap density is reduced after passivation, which in turn, suppresses the non-radiative recombination. Moreover, the UV–vis absorption spectrum of passivated film shows a slightly red shift and stronger absorption than that of the control (Fig. S3, Supporting Information) implying that the trap density of perovskite is suppressed by quinolinic acid [55].

To study the influence of QA addition and its multi-passivation effect on the photovoltaic performance, we fabricated PSCs with a configuration of ITO/PEDOT:PSS/$MAPbI_3$/$PC_{61}BM$/BCP/Ag as shown in Fig. 4a. The energy levels of individual layers in the device are shown in Fig. 4b, where that of perovskites are deduced by ultraviolet photoemission spectroscopy (UPS) (Fig. S4, Supporting Information) and optical bandgap while that of remaining layers are referenced from prior lit. Reported [56]. From the UPS measurement and optical bandgap, conduction band (CB) and valence band (VB) of pristine perovskite are −4.03 eV and −5.62 eV, respectively, while that of passivated perovskite are −3.90 eV and −5.47 eV, respectively. The higher CB of passivated perovskite (-3.90 eV) is more favorable for electron transfer into PCBM (the LUMO energy level is −4.00 eV) than that of the control film (-4.03 eV), while the higher VB of passivated perovskite is favorable for blocking the hole transfer into PCBM.

The dependence of the device performance on concentrations of QA is carefully evaluated, and the optimal concentration at 2 mg mL^{-1} yields the best performance (Fig. S5 and Table S2). To examine the multi-passivation effect of QA on device performance, the control and passivated devices with the same concentration of either QA, pyridine or acetic acid were fabricated. The *J-V* characteristics of fabricated devices and detailed electrical parameters are summarized in Fig. 4c and

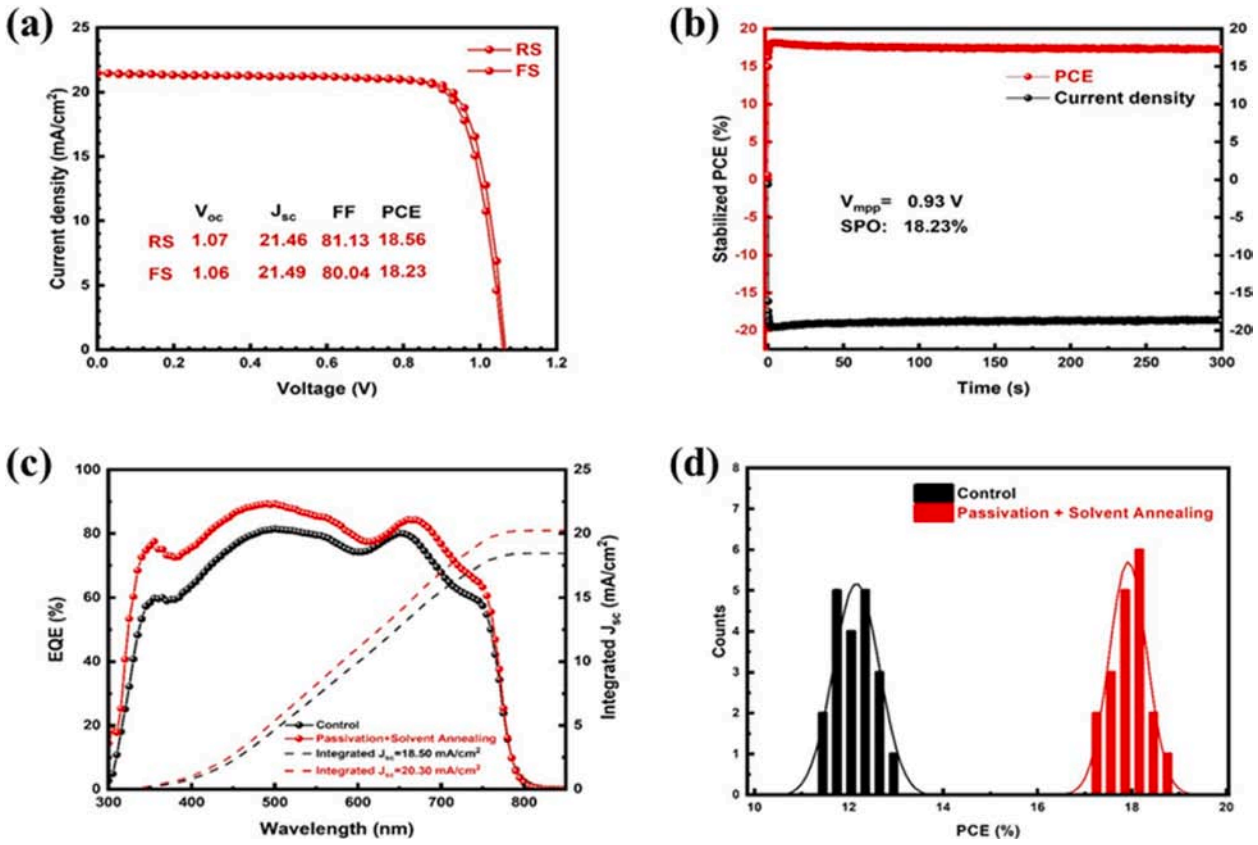

Fig. 5. (a) The *J–V* curves of champion QA + SA device. (b) The stabilized PCE measurement of the champion device. (c) EQE spectrum and integrated short-circuit current density of control and QA + SA devices. (d) PCE histograms of control and QA + SA devices from 20 devices in each category.

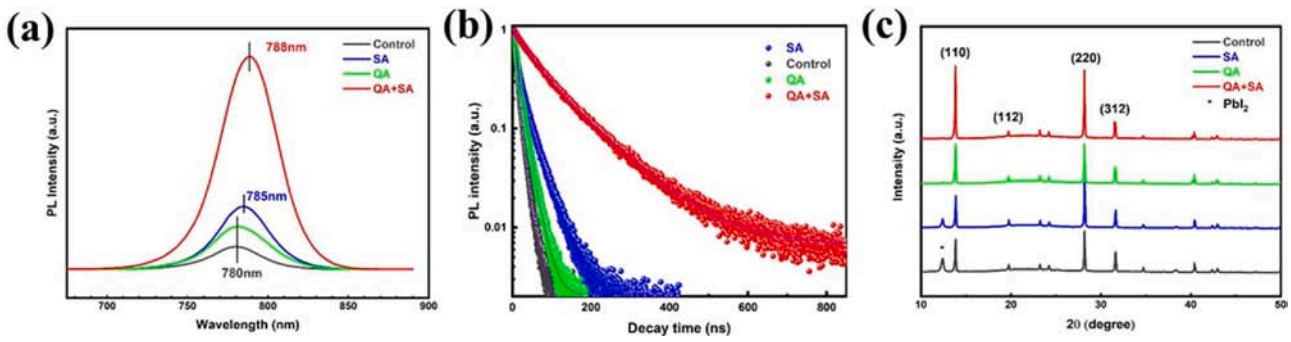

Fig. 6. (a) Steady-state PL spectra. (b) The decay curves of the TRPL intensity of perovskite films fabricated with different conditions, excited with a 450 nm laser. (c) X-ray diffractogram (XRD) of perovskite films fabricated with different conditions.

Table S3. The PCE of control device is only 12.04% with $J_{sc} = 19.58$ mA cm^{-2}, $V_{oc} = 0.82$ V and $FF = 74.57\%$, while that of passivated one with pyridine or acetic acid alone is 13.41% and 13.5% with an obvious increment in V_{oc} to 0.90 V and 0.93 V, respectively, indicating the passivation effect of pyridine and acetic acid and reduction of defects in perovskite films. However, the PCE of the QA passivated device is up to 16.4% with a significant increment of $V_{oc} = 1.05$ V. As we all known, V_{oc} is proportional to the non-radiative recombination loss caused by traps in photovoltaic device, and hence, the V_{oc} increment in QA passivated device (0.23 V) clearly indicates that the multi-passivation effect from QA is much more efficient than normal passivation effect from pyridine or acetic acid alone, in which the increment of V_{oc} is just only 0.08 V and 0.11 V, respectively.

2.3. The performance of PSCs treated with passivation and solvent annealing

It has been proved that solvent-annealing (SA) is an efficient way to optimize the morphology of the perovskite films [57]. There is mass transportation from small grains to large ones by the dissolution − recrystallization process, which follows the Ostwald ripening model [58,59]. The solvent-annealing increases the grain size of polycrystalline film and also renders high-quality film, both of which improve the performance of the perovskite solar cell [60]. The common solvents used for solvent annealing include H_2O, GBL (γ-butyrolactone), DMF and DMSO [61]. Considering that the H_2O usually leads to the degradation of $MAPbI_3$ and it is also not suitable for the device fabrication in N_2 glove box, we did not choose it for solvent-annealing. Comparing with GBL (b. p. 358.8 °C) and DMSO (b.p. 189 °C), DMF (m.p.153 °C) makes the secondary recrystallization of $MAPbI_3$ much easier to be controlled because of its weaker interactions with PbI_2, and additionally the lower boiling point makes it easier to be removed from the system. So herein we chose DMF for solvent-annealing. Firstly, we annealed the perovskite films with different amount of DMF to optimize the solvent annealing condition (Fig. S6, Supporting Information), and then combined this condition with the passivation strategy together to improve the performance of PSCs further. Secondly, to investigate the effects of processing conditions on the photovoltaic properties of devices, we fabricated the corresponding devices of PSCs (Fig. 4a) with different conditions: no special treatment (control device), passivated with QA (QA device), solvent-annealing with DMF (SA device), and combination of passivation with QA and solvent-annealing with DMF (QA + SA device) sequentially.

The *J-V* curves of the perovskite solar cells with the different processing conditions are shown in Fig. S7 and the data are summarized in Table S4. Comparing to control device, the QA one demonstrates an obvious increment of V_{oc} (1.05 V, 0.16 V higher) and the SA one displays a higher J_{sc} (20.58 mA cm^{-2}, improved about 1.35 mA cm^{-2}), while the QA + SA device yields the highest PCE of 18.56 % with a V_{oc} of 1.07 V, a J_{sc} of 21.46 mA cm^{-2}, a *FF* of 81.13% and negligible hysteresis (Fig. 5a), in which all parameters are higher than that only treated with QA or SA. External quantum efficiency (EQE) spectra of the control and QA + SA devices are characterized in the range of 300–800 nm and the integrated photocurrent densities agree well with J_{sc} values from the *J-V* curves (Fig. 5c). As shown in Fig. 5b, the QA + SA device exhibits a stabilized photocurrent and power output under continuous operation (AM1.5G illumination) at the maximum power point for 300 s. Additionally, the statistical chart from 20 devices shows good reproducibility of devices (Fig. 5d).

2.4. Optoelectronic properties and morphologies of perovskite films with different treatments

To investigate the optoelectronic properties of perovskite films fabricated with QA, SA and QA + SA treatments, the steady-state PL decay measurements are firstly conducted. As shown in Fig. 6a, the PL peak of the perovskite film becomes stronger and stronger with the treatment by QA, SA and QA + SA, and the one treated with QA + SA exhibits the strongest peak at 788 nm, which indicates that the combined method of QA + SA is much more efficient than QA or SA on reducing the trap density and forming a high-quality film. Additionally, it's interesting that the PL peak of QA film is stronger than that of the control but without any shifts, while that of the SA film is not only much stronger but also displays a little redshift (ca. 5 nm). The broader absorption range and redshift of band edge in SA film indicates that the bandgap of perovskite decreases after solvent annealing, which is consistent with higher absorption in UV–vis spectroscopy. All these results indicate that SA is more efficient to enhance the crystalline of films by recrystallization and enlarge the grain size, while QA mainly passivates the defects and accelerates the formation of small crystals of perovskite and also can enhance the recrystallization drastically when combined with SA.

Secondly, time-resolved photoluminescence (TRPL) measurements were carried out to investigate impacts by treatments with QA, SA and QA + SA, respectively, on the charge carrier recombination dynamic (Fig. 6b). The TRPL decay curves are fitted by using bi-exponential decay function as shown in equation (1), and the average carrier lifetime τ_{avg} was calculated by equation (2).

$$I(t) = A_1 \exp\left(-\frac{t}{\tau_1}\right) + A_2 \exp\left(-\frac{t}{\tau_2}\right) \quad (1)$$

$$\tau_{avg} = (A_1\tau_1^2 + A_2\tau_2^2)/(A_1\tau_1 + A_2\tau_2) \quad (2)$$

where the time constant τ_1 represents the bimolecular recombination of photo-generated free carriers, τ_2 represents the trap-assisted recombination induced by defects, τ_{avg} represents the average of τ_1 and τ_2, and A_1 and A_2 represent PL decay amplitudes [62]. The results are summarized in Table S5, and it is obvious that the combined method with QA + SA demonstrates the most efficient for suppression of bimolecular and trap-assisted combinations with τ_1 of 43.01 ns, τ_2 of 114.37 ns, and τ_{avg}

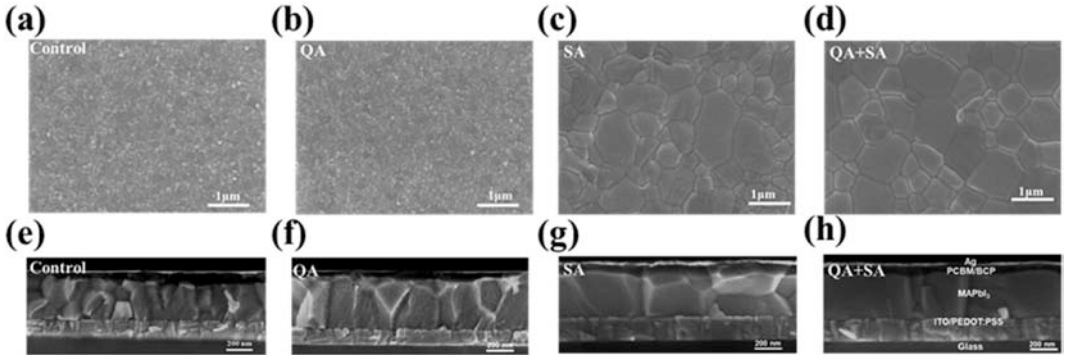

Fig. 7. Top-view and cross-section scanning electron microscopy (SEM) images of perovskite films with different treatments.

of 99.38 ns. Comparing with QA, the treatment SA can much more efficient on reducing the trap-assisted combination with a higher τ_2 of 30.75 ns and τ_{avg} of 24.51 ns. All these results matched very well with XRD and SEM, which are discussed later.

To explore the impact of different treatments on the crystallinity of perovskite, we compared the X-ray diffraction (XRD) patterns of perovskite films treated with different conditions. As shown in Fig. 6c, with different treatments, the peak intensities of (1 1 0) at 14.1° and (2 2 0) at 28.4° increase relative to that of (3 1 2) at 31.86°, respectively. Comparing with the control film, the SA treated film displays a strong peak of (2 2 0) at 28.4°, another moderately strong peak of (1 1 0) at 14.1°, and a small peak of (0 0 1) at 12.5° that represents PbI_2 cubic phase in perovskite; while QA treated film demonstrates strong peak of (1 1 0) and (2 2 0) with similar intensity and a negligible peak of PbI_2. The QA + SA treated film yields the strongest peaks of (1 1 0) and (2 2 0) among the different films without the peak of PbI_2. It is known that the moderate excess of PbI_2 preferentially fills grain boundary defects, while excess PbI_2 will become non-radiative recombination centers, leading to decrements of V_{oc}. [63] All these results indicate that QA treatment yield purer perovskite without PbI_2 residue, leading to a sharp increase of V_{oc}, while the SA treatment mainly enhances the crystalline of perovskite film but with excess PbI_2 residue, yielding a slight increase of V_{oc} but a sharp increase of J_{sc}. So the combined QA + SA treatment dramatically improves both the purity and crystalline of perovskite, which leads to a high performance of PSCs.

The top-view and cross-section scanning electron microscopy (SEM) measurements were carried out to explore the influence of different treatments on morphologies of perovskite layer (Fig. 7). The statistical distributions of corresponding grain size (Fig. S8, Supporting Information) reveal that the grain sizes are in increasing order of control film, QA, SA and QA + SA film with average size of 205 nm, 278 nm, 835 nm and 1013 nm, respectively. Noteworthy, the average grain size of QA + SA film (~1013 nm) is hardly achievable, especially for the perovskite film fabricated on PEDOT:PSS.

As shown in Fig. 7 and Fig. S8, the QA treated film shows a little increment of grain size both on the surface and in the bulk of perovskite layer, while the SA treated film displays more than 4 times bigger grain size and high crystalline with some grain boundaries compared with the control film. The QA + SA treated film demonstrates the biggest grains with grain size over 1 μm and few grain boundaries. In addition, atomic force microscopy (AFM) was performed to examine the surface morphology. As shown in Fig. S9, the RMS roughness of control, QA, SA and QA + SA are 26.64, 11.47, 22.56 and 16.74 nm for the respectively. The control film displays much more pinholes than that of QA, SA and QA + SA. It's worth noting that QA can efficiently reduce pinholes and the roughness, while SA demonstrates less efficient on reducing pinholes and roughness of films. These may attribute to the excess PbI_2 residue and the much easier evaporation of MA, HI, MAI and other components with low boiling points in films treated with SA alone. So, after treated with QA + SA, the perovskite films with bigger grain size, higher crystalline but less pinholes are beneficial for the increments of V_{oc} and J_{sc} of the corresponding devices, [64-67] which contributes to the enhancement of both efficiency and stability of PSCs [68].

To evaluate the trap density of different perovskite devices, dark *J-V* curves of hole-only device with the structure of ITO/PEDOT:PSS/perovskite/Au were measured by the space-charge-limited current (SCLC) method [69]. The defect density was calculated according to the equation (3)

$$V_{TFL} = qN_tL^2/2\varepsilon_0\varepsilon_r \quad (3)$$

where V_{TFL} represents the onset voltage of trap filled limit, q is electric charge (1.6×10^{-19}C), L is the thickness of the active layer, ε_0 is the vacuum permittivity (8.85×10^{-14}F/cm) and ε_r is dielectric constant of perovskite (taken as the value of 32 for $MAPbI_3$ from the previous report [66]) As shown in Fig. S10a and b, the N_{trap} of the QA + SA treated film and pristine perovskite film are ~ 1.55×10^{16} cm^{-3} and ~ 2.43×10^{16} cm^{-3}, respectively, and the lower N_{trap} of the perovskite film contributes to the increment of V_{oc}. [70] Furthermore, electrical impedance spectroscopy revealed that recombination resistance (R_{rec}) increases in the device fabricated by combined method as shown in Fig. S10c. Meanwhile, the leakage current of the QA + SA device is smaller than that of control device from the dark *J-V* curve of the PSCs (Fig. S11, Supporting Information), indicating that the non-radiative recombination is suppressed drastically in QA + SA device [71,72].

To further study the V_{oc} of the incorporated PSCs, recombination mechanism is attained via fitting the V_{oc} varied logarithmically with light intensity (ln(I)) relationship based on equation (4).

$$V_{oc} = nkT/q\ln(I) \quad (4)$$

where n is ideal factor, k is the Boltzmann constant, T is absolute temperature, and q is the electron charge. In principle, a slope approximately in the order of kT/q is a signal that bimolecular recombination is dominant without trap-assisted recombination, while a stronger dependence of V_{oc} on ln(I) with a slope of 2 kT/q is identified that trap-assisted recombination become serious. As shown in Fig. S10d, the fitting value of n is 1.47 for QA + SA device, which is much smaller than that of the control one (1.98), indicating that the combined method of QA + SA can effectively suppress the trap-assisted Shockley-Read-Hall recombination [73]. Thus, the high-quality perovskite film with low trap density by the combined method contributes to V_{oc} enhancement of device.

2.5. Humidity stability of the devices

Besides PCE, the device stability is another key parameter for high-performance perovskite solar cell [74]. With our combined method of QA + SA, high-quality of perovskite films with large gain size over 1 μm and uniform crystals are formed, leading to less grain boundaries and defects in the film. These results usually mean not only the improvement of PCE, but also the enhancement of stability of PSCs. To prove that, we

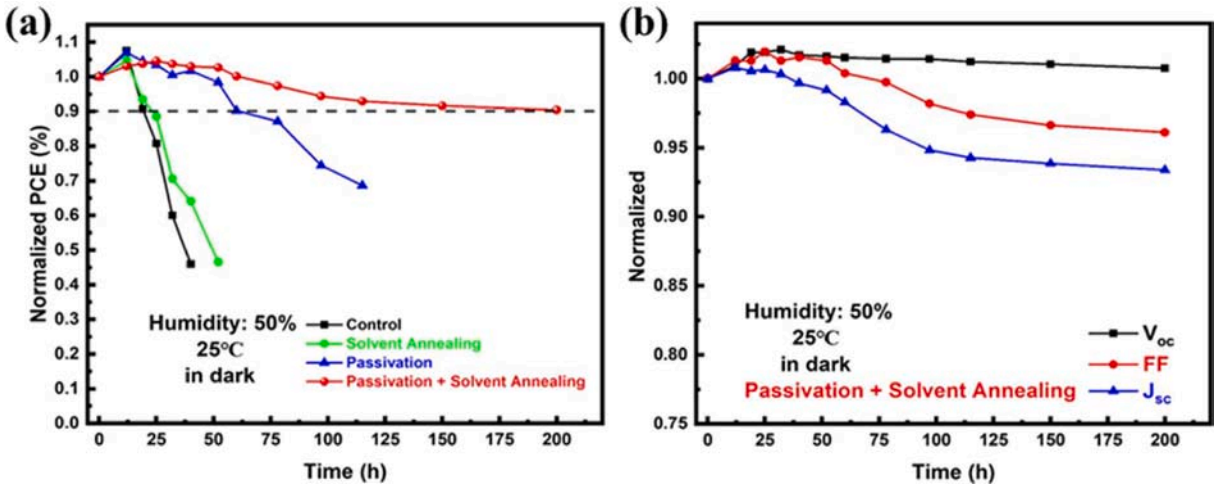

Fig. 8. (a) Stability test of the devices fabricated by different processing conditions. (b) The variation in photovoltaic parameters of QA + SA device over time.

firstly tested the changes of water contact angle of perovskite films with different treatments. As shown in Fig. S12, after treating with QA or SA alone, the contact angle of perovskite film increases to 56° or 51° from 40° (the control one), while the contact angle of perovskite film further increases to 66° after treating with QA + SA, indicating that the treated films have higher moisture resistance and the corresponding device should demonstrate a better stability [75]. So the stabilities of the control, QA, SA and QA + SA, respectively, are tested in air condition with ~50% relative humidity (RH) at room temperature. The PCE of QA + SA device remains more than 90% of its initial value with a negligible decrease of V_{oc} after keeping in the condition for more than 200 h, ~8 times more stable than the control device (Fig. 8). It is worth mentioning that the stability of SA device is not improved obviously while that of QA device is improved by 3 times, which may attribute to the multi-passivation effect of QA. All these findings demonstrate a great advantage of the combined method of QA and SA compared with the QA or SA treatment alone.

3. Conclusion

In conclusion, we have demonstrated the multi-passivation effect in perovskite film by employing quinolinic acid (QA) as additive in the precursor. The strong interaction between QA and perovskite precursors in solution phase prevents the formation of MA^+ or I^- vacancies and metallic Pb_0 clusters, which benefits for the preparation of high-quality perovskite film with low trap density. Moreover, pyridine and dicarboxylic acid groups in QA passivate the positively charged defects such as undercoordinated Pb^{2+}, I^- vacancies and metallic Pb_0 cluster by donating lone pair electrons from N and O atoms through Lewis base passivation mechanism. With the combined sequential strategy of QA + SA, we drastically improve the quality of perovskite film by enlarging grain size over 1 μm and reducing defects and pinholes. As a result, the PSC fabricated with the combined method demonstrates an excellent humidity stability and yields a PCE of 18.56% with 20% and 11.6% increment of V_{oc} and J_{sc} respectively. To our best knowledge, it is the highest reported PCE for inverted PSCs with undoped PEDOT:PSS. Therefore, our work indicates that the new combined strategy of multi-passivation with QA and solvent annealing with DMF has a significant potential for highly efficient and stable inverted planar PSCs.

Declaration of Competing Interest

The authors declare that they have no known competing financial interests or personal relationships that could have appeared to influence the work reported in this paper.

Acknowledgements

Prof. G. Li thanks for the general supported by the National Key R&D Program of China (2017YFA0204704), the National Natural Science Foundation of China (51773091, 22075140), Six Talent Peaks Project in Jiangsu Province (XCL-026) and the Open Project Program of Wuhan National Laboratory for Optoelectronics (NO. 2020WNLOKF010). Prof. A. K. K. Kyaw would like to thank support from National Natural Science Foundation of China (Grant No. 62150610496), Guangdong Basic and Applied Basic Research Foundation (2020A1515010916), and Department of Education of Guangdong Province University Innovation Foundation (2021KTSCX107). .

Appendix A. Supplementary data

Supplementary data to this article can be found online at https://doi.org/10.1016/j.cej.2022.135107.

References

[1] E.H. Jung, N.J. Jeon, E.Y. Park, C.S. Moon, T.J. Shin, T.-Y. Yang, J.H. Noh, J. Seo, Efficient, stable and scalable perovskite solar cells using poly(3-hexylthiophene), Nature 567 (7749) (2019) 511–515.
[2] D. Koo, Y. Cho, U. Kim, G. Jeong, J. Lee, J. Seo, C. Yang, H. Park, High-Performance Inverted Perovskite Solar Cells with Operational Stability via n-Type Small Molecule Additive-Assisted Defect Passivation, Adv. Energy Mater. 10 (46) (2020) 2001920, https://doi.org/10.1002/aenm.v10.4610.1002/aenm.202001920.
[3] Z. He, J. Xiong, Q. Dai, B. Yang, J. Zhang, S.i. Xiao, High-performance inverted perovskite solar cells using 4-diaminomethylbenzoic as a passivant, Nanoscale 12 (12) (2020) 6767–6775.
[4] W. Zhang, Development of high-performance inverted perovskite solar cells, J. Photonics Energy 11893 (2021) 118930E.
[5] C. Wang, Z. Su, L. Chen, H. Zhang, W. Hui, D. Liang, G. Zheng, L. Zhang, Z. Tang, W. Wen, J. Tang, Q. Huang, F. Song, Q. Chen, X. Gao, MoO_3 doped PTAA for high-performance inverted perovskite solar cells, Appl. Surf. Sci. 571 (2022) 151301–151308.
[6] C.N. Brodsky, D.K. Bediako, C. Shi, T.P. Keane, C. Costentin, S.J.L. Billinge, D. G. Nocera, Proton-Electron Conductivity in Thin Films of a Cobalt-Oxygen Evolving Catalyst, ACS Appl. Energy Mater. 2 (1) (2019) 3–12.
[7] K. Yang, Q. Liao, J. Huang, Z. Zhang, M. Su, Z. Chen, Z. Wu, D. Wang, Z. Lai, H. Y. Woo, Y. Cao, P. Gao, X. Guo, Intramolecular Noncovalent Interaction-Enabled Dopant-Free Hole-Transporting Materials for High-Performance Inverted Perovskite Solar Cells, Angew. Chem. Int. Ed. 61 (2) (2022), https://doi.org/10.1002/anie.v61.210.1002/anie.202113749.
[8] Q.i. Xiao, J. Tian, Q. Xue, J. Wang, B. Xiong, M. Han, Z. Li, Z. Zhu, H.-L. Yip, Z. Li, Dopant-Free Squaraine-Based Polymeric Hole-Transporting Materials with Comprehensive Passivation Effects for Efficient All-Inorganic Perovskite Solar Cells, Angew. Chem. Int. Ed. 58 (49) (2019) 17724–17730.
[9] K. Jiang, J. Wang, F. Wu, Q. Xue, Q. Yao, J. Zhang, Y. Chen, G. Zhang, Z. Zhu, H. e. Yan, L. Zhu, H.-L. Yip, Dopant-Free Organic Hole-Transporting Material for Efficient and Stable Inverted All-Inorganic and Hybrid Perovskite Solar Cells, Adv.

Mater. 32 (16) (2020) 1908011, https://doi.org/10.1002/adma.v32.1610.1002/adma.201908011.
[10] T.A.S. Doherty, A.J. Winchester, S. Macpherson, D.N. Johnstone, V. Pareek, E. M. Tennyson, S. Kosar, F.U. Kosasih, M. Anaya, M. Abdi-Jalebi, Z. Andaji-Garmaroudi, E.L. Wong, J. Madéo, Y.-H. Chiang, J.-S. Park, Y.-K. Jung, C. E. Petoukhoff, G. Divitini, M.K.L. Man, C. Ducati, A. Walsh, P.A. Midgley, K. M. Dani, S.D. Stranks, Performance-limiting nanoscale trap clusters at grain junctions in halide perovskites, Nature 580 (7803) (2020) 360–366.
[11] S. Bai, P. Da, C. Li, Z. Wang, Z. Yuan, F. Fu, M. Kawecki, X. Liu, N. Sakai, J.-W. Wang, S. Huettner, S. Buecheler, M. Fahlman, F. Gao, H.J. Snaith, Planar perovskite solar cells with long-term stability using ionic liquid additives, Nature 571 (7764) (2019) 245–250.
[12] C. Bi, Q. Wang, Y. Shao, Y. Yuan, Z. Xiao, J. Huang, Non-wetting surface-driven high-aspect-ratio crystalline grain growth for efficient hybrid perovskite solar cells, Nat. Commun. 6 (2015) 7747–7753.
[13] Y. Li, H. Wu, W. Qi, X. Zhou, J. Li, J. Cheng, Y. Zhao, Y. Li, X. Zhang, Passivation of defects in perovskite solar cell: From a chemistry point of view, Nano Energy 77 (2020) 105237–105264.
[14] Q. Sun, W.-J. Yin, Thermodynamic Stability Trend of Cubic Perovskites, J. Am. Chem. Soc. 139 (42) (2017) 14905–14908.
[15] X. Lin, D. Cui, X. Luo, C. Zhang, Q. Han, Y. Wang, L. Han, Efficiency progress of inverted perovskite solar cells, Energy Environ. Sci. 13 (11) (2020) 3823–3847.
[16] Y. Rong, Y. Hu, A. Mei, H. Tan, M.I. Saidaminov, S.I. Seok, M.D. McGehee, E. H. Sargent, H. Han, Challenges for commercializing perovskite solar cells, Science 361 (6408) (2018), https://doi.org/10.1126/science:aat8235.
[17] H. Min, D.Y. Lee, J. Kim, G. Kim, K.S. Lee, J. Kim, M.J. Paik, Y.K. Kim, K.S. Kim, M. G. Kim, T.J. Shin, S. Il Seok, Perovskite solar cells with atomically coherent interlayers on SnO_2 electrodes, Nature 598 (7881) (2021) 444–450.
[18] G. Kim, H. Min, K.S. Lee, D.Y. Lee, S.M. Yoon, S.I. Seok†, Impact of strain relaxation on performance of a-formamidinium lead iodide perovskite solar cells, Science 370 (2020) 108–112.
[19] J. Jeong, M. Kim, J. Seo, H. Lu, P. Ahlawat, A. Mishra, Y. Yang, M.A. Hope, F. T. Eickemeyer, M. Kim, Y.J. Yoon, I.W. Choi, B.P. Darwich, S.J. Choi, Y. Jo, J. H. Lee, B. Walker, S.M. Zakeeruddin, L. Emsley, U. Rothlisberger, A. Hagfeldt, D. S. Kim, M. Gratzel, J.Y. Kim, Pseudo-halide anion engineering for alpha-$FAPbI_3$ perovskite solar cells, Nature 592 (2021) 381–385.
[20] Xiaoyu Yang, Yunqi Fu, Rui Su, Yifan Zheng, Yuzhuo Zhang, Wenqiang Yang, Maotao Yu, Peng Chen, Yanju Wang, Jiang Wu, Deying Luo, Yongguang Tu, Lichen Zhao, Qihuang Gong, Rui Zhu, Superior Carrier Lifetimes Exceeding 6 μs in Polycrystalline Halide Perovskites, Adv. Mater. 32 (39) (2020) 2002585, https://doi.org/10.1002/adma.v32.3910.1002/adma.202002585.
[21] Jason J. Yoo, Gabkyung Seo, Matthew R. Chua, Tae Gwan Park, Yongli Lu, Fabian Rotermund, Young-Ki Kim, Chan Su Moon, Nam Joong Jeon, Juan-Pablo Correa-Baena, Vladimir Bulović, Seong Sik Shin, Moungi G. Bawendi, Jangwon Seo, Efficient perovskite solar cells via improved carrier management, Nature 590 (7847) (2021) 587–593.
[22] Qi Jiang, Yang Zhao, Xingwang Zhang, Xiaolei Yang, Yong Chen, Zema Chu, Qiufeng Ye, Xingxing Li, Zhigang Yin, Jingbi You, Surface passivation of perovskite film for efficient solar cells, Nat. Photonics 13 (7) (2019) 460–466.
[23] Xiaoxi Wu, M. Tuan Trinh, Daniel Niesner, Haiming Zhu, Zachariah Norman, Jonathan S. Owen, Omer Yaffe, Bryan J. Kudisch, X.-Y. Zhu, Trap States in Lead Iodide Perovskites, J. Am. Chem. Soc. 137 (5) (2015) 2089–2096.
[24] Run Long, Jin Liu, Oleg V. Prezhdo, Unravelling the Effects of Grain Boundary and Chemical Doping on Electron-Hole Recombination in $CH_3NH_3PbI_3$ Perovskite by Time-Domain Atomistic Simulation, J. Am. Chem. Soc. 138 (11) (2016) 3884–3890.
[25] Fei Zhang, Kai Zhu, Additive Engineering for Efficient and Stable Perovskite Solar Cells, Adv. Energy Mater. 10 (13) (2020) 1902579, https://doi.org/10.1002/aenm.v10.1310.1002/aenm.201902579.
[26] Pengjun Zhao, Byeong Jo Kim, Xiaodong Ren, Dong Geon Lee, Gi Joo Bang, Jae Bum Jeon, Won Bin Kim, Hyun Suk Jung, Antisolvent with an Ultrawide Processing Window for the One-Step Fabrication of Efficient and Large-Area Perovskite Solar Cells, Adv. Mater. 30 (49) (2018) 1802763, https://doi.org/10.1002/adma.v30.4910.1002/adma.201802763.
[27] Dong-Ho Kang, So-Yeon Kim, Jin-Wook Lee, Nam-Gyu Park, Efficient surface passivation of perovskite films by a post-treatment method with a minimal dose, J. Mater. Chem. A 9 (6) (2021) 3441–3450.
[28] Taotao Li, Yufeng Pan, Ze Wang, Yingdong Xia, Yonghua Chen, Wei Huang, Additive engineering for highly efficient organic–inorganic halide perovskite solar cells: recent advances and perspectives, J. Mater. Chem. A 5 (25) (2017) 12602–12652.
[29] Apurba Mahapatra, Daniel Prochowicz, Mohammad Mahdi Tavakoli, Suverna Trivedi, Pawan Kumar, Pankaj Yadav, A review of aspects of additive engineering in perovskite solar cells, J. Mater. Chem. A 8 (1) (2020) 27–54.
[30] Feilong Cai, Yu Yan, Jiaxu Yao, Pang Wang, Hui Wang, Robert S. Gurney, Dan Liu, Tao Wang, Ionic Additive Engineering Toward High-Efficiency Perovskite Solar Cells with Reduced Grain Boundaries and Trap Density, Adv. Funct. Mater. 28 (34) (2018) 1801985, https://doi.org/10.1002/adfm.201801985.
[31] Deng Wang, Wenjing Li, Zhenbo Du, Guodong Li, Weihai Sun, Jihuai Wu, Zhang Lan, Highly Efficient CsPbBr 3 Planar Perovskite Solar Cells via Additive Engineering with NH4SCN, ACS Appl. Mater. Interfaces 12 (9) (2020) 10579–10587.
[32] Yongzhen Wu, Fengxian Xie, Han Chen, Xudong Yang, Huimin Su, Molang Cai, Zhongmin Zhou, Takeshi Noda, Liyuan Han, Thermally Stable MAPbI3 Perovskite Solar Cells with Efficiency of 19.19% and Area over 1 cm^2 achieved by Additive Engineering, Adv. Mater. 29 (28) (2017) 1701073, https://doi.org/10.1002/adma.v29.2810.1002/adma.201701073.
[33] J. Xu, A. Buin, A.H. Ip, W. Li, O. Voznyy, R. Comin, M. Yuan, S. Jeon, Z. Ning, J. J. McDowell, P. Kanjanaboos, J.P. Sun, X. Lan, L.N. Quan, D.H. Kim, I.G. Hill, P. Maksymovych, E.H. Sargent, Perovskite-fullerene hybrid materials suppress hysteresis in planar diodes, Nat. Commun. 6 (2015) 7081–7088.
[34] Yuze Lin, Bo Chen, Fuwen Zhao, Xiaopeng Zheng, Yehao Deng, Yuchuan Shao, Yanjun Fang, Yang Bai, Chunru Wang, Jinsong Huang, Matching Charge Extraction Contact for Wide-Bandgap Perovskite Solar Cells, Adv. Mater. 29 (26) (2017) 1700607, https://doi.org/10.1002/adma.v29.2610.1002/adma.201700607.
[35] P. Qin, G. Yang, Z.W. Ren, S.H. Cheung, S. So, L. Chen, J. Hao, J. Hou, G. Li, Stable and Efficient Organo-Metal Halide Hybrid Perovskite Solar Cells via pi-Conjugated Lewis Base Polymer Induced Trap Passivation and Charge Extraction, Adv. Mater. 30 (2018) 1706126–1706137.
[36] Qiwei Han, Yusong Bai, Jie Liu, Ke-zhao Du, Tianyang Li, Dong Ji, Yihao Zhou, Changyong Cao, Donghyeop Shin, Jie Ding, Aaron D. Franklin, Jeffrey T. Glass, Jinsong Hu, Michael J. Therien, Jie Liu, David B. Mitzi, Additive engineering for high-performance room-temperature-processed perovskite absorbers with micron-size grains and microsecond-range carrier lifetimes, Energy Environ. Sci. 10 (11) (2017) 2365–2371.
[37] Dominik J. Kubicki, Daniel Prochowicz, Albert Hofstetter, Shaik M. Zakeeruddin, Michael Grätzel, Lyndon Emsley, Phase Segregation in Cs-, Rb- and K-Doped Mixed-Cation (MA)x(FA)1–xPbI3 Hybrid Perovskites from Solid-State NMR, J. Am. Chem. Soc. 139 (40) (2017) 14173–14180.
[38] Dae-Yong Son, Seul-Gi Kim, Ja-Young Seo, Seon-Hee Lee, Hyunjung Shin, Donghwa Lee, Nam-Gyu Park, Universal Approach toward Hysteresis-Free Perovskite Solar Cell via Defect Engineering, J. Am. Chem. Soc. 140 (4) (2018) 1358–1364.
[39] G. Nan, X. Zhang, M. Abdi-Jalebi, Z. Andaji-Garmaroudi, S.D. Stranks, G. Lu, D. Beljonne, How Methylammonium Cations and Chlorine Dopants Heal Defects in Lead Iodide Perovskites, Adv. Energy Mater. 8 (2018) 1702754.
[40] Hairen Tan, Ankit Jain, Oleksandr Voznyy, Xinzheng Lan, F. Pelayo García de Arquer, James Z. Fan, Rafael Quintero-Bermudez, Mingjian Yuan, Bo Zhang, Yicheng Zhao, Fengjia Fan, Peicheng Li, Li Na Quan, Yongbiao Zhao, Zheng-Hong Lu, Zhenyu Yang, Sjoerd Hoogland, Edward H. Sargent, Efficient and stable solution-processed planar perovskite solar cells via contact passivation, Science 355 (6326) (2017) 722–726.
[41] Xianqiang Li, Wenhui Li, Yijie Yang, Xue Lai, Qiang Su, Dan Wu, Gongqiang Li, Kai Wang, Shuming Chen, Xiao Wei Sun, Aung Ko Ko Kyaw, Defects Passivation With Dithienobenzodithiophene-based π-conjugated Polymer for Enhanced Performance of Perovskite Solar Cells, Sol. RRL 3 (6) (2019) 1900029, https://doi.org/10.1002/solr.v3.610.1002/solr.201900029.
[42] W. Li, X. Lai, F. Meng, G. Li, K. Wang, A.K.K. Kyaw, X. Sun, Efficient defect-passivation and charge-transfer with interfacial organophosphorus ligand modification for enhanced performance of perovskite solar cells, Sol. Energy Mater. Sol. Cells 211 (2020) 110527–110536.
[43] Xue Lai, Fei Meng, Qian-Qian Zhang, Kai Wang, Gongqiang Li, Yaping Wen, Haibo Ma, Wenhui Li, Xianqiang Li, Aung Ko Ko Kyaw, Kai Wang, Xiao Wei Sun, Mengzhen Du, Xiao Guo, Jianpu Wang, Wei Huang, A Bifunctional Saddle-Shaped Small Molecule as a Dopant-Free Hole Transporting Material and Interfacial Layer for Efficient and Stable Perovskite Solar Cells, Sol. RRL 3 (5) (2019) 1900011, https://doi.org/10.1002/solr.v3.510.1002/solr.201900011.
[44] Xiaopeng Zheng, Yehao Deng, Bo Chen, Haotong Wei, Xun Xiao, Yanjun Fang, Yuze Lin, Zhenhua Yu, Ye Liu, Qi Wang, Jinsong Huang, Dual Functions of Crystallization Control and Defect Passivation Enabled by Sulfonic Zwitterions for Stable and Efficient Perovskite Solar Cells, Adv. Mater. 30 (52) (2018) 1803428, https://doi.org/10.1002/adma.v30.5210.1002/adma.201803428.
[45] K. Jiang, F. Wu, G. Zhang, P.C.Y. Chow, C. Ma, S. Li, K.S. Wong, L. Zhu, H. Yan, Inverted planar perovskite solar cells based on CsI-doped PEDOT:PSS with efficiency beyond 20% and small energy loss, J. Mater. Chem. A 7 (2019) 21662–21667.
[46] F. Wu, K. Yan, H. Wu, B. Niu, Z. Liu, Y. Li, L. Zuo, H. Chen, Tuning interfacial chemical interaction for high-performance perovskite solar cell with PEDOT:PSS as hole transporting layer, J. Mater. Chem. A 9 (2021) 14920–14927.
[47] Jiangzhao Chen, Yuli Xiong, Yaoguang Rong, Anyi Mei, Yusong Sheng, Pei Jiang, Yue Hu, Xiong Li, Hongwei Han, Solvent effect on the hole-conductor-free fully printable perovskite solar cells, Nano Energy 27 (2016) 130–137.
[48] Bert Conings, Jeroen Drijkoningen, Nicolas Gauquelin, Aslihan Babayigit, Jan D'Haen, Lien D'Olieslaeger, Anitha Ethirajan, Jo Verbeeck, Jean Manca, Edoardo Mosconi, Filippo De Angelis, Hans-Gerd Boyen, Intrinsic Thermal Instability of Methylammonium Lead Trihalide Perovskite, Adv. Energy Mater. 5 (15) (2015) 1500477, https://doi.org/10.1002/aenm.201500477.
[49] Yifan Lv, Hui Zhang, Jinpei Wang, Libao Chen, Lifang Bian, Zhongfu An, Zongyao Qian, Guoqi Ren, Jie Wu, Frank Nüesch, Wei Huang, All-in-One Deposition to Synergistically Manipulate Perovskite Growth for High-Performance Solar Cell, Research 2020 (2020) 1–10.
[50] Ying-Chiao Wang, Junwei Chang, Liping Zhu, Xiaodong Li, Changjian Song, Junfeng Fang, Electron-Transport-Layer-Assisted Crystallization of Perovskite Films for High-Efficiency Planar Heterojunction Solar Cells, Adv. Funct. Mater. 28 (9) (2018) 1706317, https://doi.org/10.1002/adfm.v28.910.1002/adfm.201706317.
[51] D. Bi, C. Yi, J. Luo, J.D. Décoppet, F. Zhang, S.M. Zakeeruddin, X. Li, A. Hagfeldt, M. Grätzel, Polymer-templated nucleation and crystal growth of perovskite films for solar cells with efficiency greater than 21%, Nat. Energy 1 (2016) 16142–16146.

[52] Yulei Wu, Xiaodong Li, Sheng Fu, Li Wan, Junfeng Fang, Efficient methylammonium lead trihalide perovskite solar cells with chloroformamidinium chloride (Cl-FACl) as an additive, J. Mater. Chem. A 7 (14) (2019) 8078–8084.
[53] J. Yang, Q. Cao, Z. He, X. Pu, T. Li, B. Gao, X. Li, The poly(styrene-co-acrylonitrile) polymer assisted preparation of high-performance inverted perovskite solar cells with efficiency exceeding 22%, Nano Energy 82 (2021) 105731–105738.
[54] Qi Cao, Jiabao Yang, Tong Wang, Yuke Li, Xingyu Pu, Junsong Zhao, Yixin Zhang, Hui Zhou, Xiaoqiang Li, Xuanhua Li, Star-polymer multidentate-cross-linking strategy for superior operational stability of inverted perovskite solar cells at high efficiency, Energy Environ. Sci. 14 (10) (2021) 5406–5415.
[55] Xiaodong Li, Wenxiao Zhang, Wenjun Zhang, Hai-Qiao Wang, Junfeng Fang, Spontaneous grain polymerization for efficient and stable perovskite solar cells, Nano Energy 58 (2019) 825–833.
[56] Xue Lai, Mengzhen Du, Fei Meng, Gongqiang Li, Wenhui Li, Aung Ko Ko Kyaw, Yaping Wen, Chungen Liu, Haibo Ma, Ren Zhang, Dongyu Fan, Xiao Guo, Yunhao Wang, Hongru Ji, Kai Wang, Xiao Wei Sun, Jianpu Wang, Wei Huang, High-Performance Inverted Planar Perovskite Solar Cells Enhanced by Thickness Tuning of New Dopant-Free Hole Transporting Layer, Small 15 (49) (2019) 1904715, https://doi.org/10.1002/smll.v15.4910.1002/smll.201904715.
[57] Liuwen Tian, Wenfeng Zhang, Hua Yu, Changtao Peng, Hanying Mao, Yuepeng Li, Qiyun Wang, Yuelong Huang, Post-treatment of Perovskite Films toward Efficient Solar Cells via Mixed Solvent Annealing, ACS Appl. Energy Mater. 2 (7) (2019) 4954–4963.
[58] Xiaobing Cao, Lili Zhi, Yahui Li, Fei Fang, Xian Cui, Lijie Ci, Kongxian Ding, Jinquan Wei, Fabrication of Perovskite Films with Large Columnar Grains via Solvent-Mediated Ostwald Ripening for Efficient Inverted Perovskite Solar Cells, ACS Appl. Energy Mater. 1 (2) (2018) 868–875.
[59] Xu Sun, Chunfu Zhang, Jingjing Chang, Haifeng Yang, He Xi, Gang Lu, Dazheng Chen, Zhenhua Lin, Xiaoli Lu, Jincheng Zhang, Yue Hao, Mixed-solvent-vapor annealing of perovskite for photovoltaic device efficiency enhancement, Nano Energy 28 (2016) 417–425.
[60] Pengyun Liu, Wei Wang, Shaomin Liu, Huagui Yang, Zongping Shao, Fundamental Understanding of Photocurrent Hysteresis in Perovskite Solar Cells, Adv. Energy Mater. 9 (13) (2019) 1803017, https://doi.org/10.1002/aenm.v9.1310.1002/aenm.201803017.
[61] Jiang Liu, Cheng Gao, Xulin He, Qinyan Ye, Liangqi Ouyang, Daming Zhuang, Cheng Liao, Jun Mei, Woonming Lau, Improved Crystallization of Perovskite Films by Optimized Solvent Annealing for High Efficiency Solar Cell, ACS Appl. Mater. Interfaces 7 (43) (2015) 24008–24015.
[62] Tianhao Wu, Yanbo Wang, Xing Li, Yongzhen Wu, Xiangyue Meng, Danyu Cui, Xudong Yang, Liyuan Han, Efficient Defect Passivation for Perovskite Solar Cells by Controlling the Electron Density Distribution of Donor-π-Acceptor Molecules, Adv. Energy Mater. 9 (17) (2019) 1803766, https://doi.org/10.1002/aenm.v9.1710.1002/aenm.201803766.
[63] T. Jesper Jacobsson, Juan-Pablo Correa-Baena, Elham Halvani Anaraki, Bertrand Philippe, Samuel D. Stranks, Marine E.F. Bouduban, Wolfgang Tress, Kurt Schenk, Joël Teuscher, Jacques-E. Moser, Håkan Rensmo, Anders Hagfeldt, Unreacted PbI_2 as a Double-Edged Sword for Enhancing the Performance of Perovskite Solar Cells, J. Am. Chem. Soc. 138 (32) (2016) 10331–10343.
[64] X. Xu, Z. Liu, Z. Zuo, M. Zhang, Z. Zhao, Y. Shen, H. Zhou, Q. Chen, Y. Yang, M. Wang, Hole selective NiO contact for efficient perovskite solar cells with carbon electrode, Nano Lett. 15 (2015) 2402.
[65] Tze-Bin Song, Qi Chen, Huanping Zhou, Chengyang Jiang, Hsin-Hua Wang, Yang (Michael) Yang, Yongsheng Liu, Jingbi You, Yang Yang, Perovskite solar cells: film formation and properties, J. Mater. Chem. A 3 (17) (2015) 9032–9050.
[66] Banavoth Murali, Emre Yengel, Chen Yang, Wei Peng, Erkki Alarousu, Osman M. Bakr, Omar F. Mohammed, The Surface of Hybrid Perovskite Crystals: A Boon or Bane, ACS Energy Lett. 2 (4) (2017) 846–856.
[67] M. Nam, M. Cha, H.H. Lee, K. Hur, K.T. Lee, J. Yoo, I.K. Han, S.J. Kwon, D.H. Ko, Long-term efficient organic photovoltaics based on quaternary bulk heterojunctions, Nat. Commun. 8 (2017) 14068–14077.
[68] Xiaopeng Zheng, Yi Hou, Chunxiong Bao, Jun Yin, Fanglong Yuan, Ziru Huang, Kepeng Song, Jiakai Liu, Joel Troughton, Nicola Gasparini, Chun Zhou, Yuanbao Lin, Ding-Jiang Xue, Bin Chen, Andrew K. Johnston, Nini Wei, Mohamed Nejib Hedhili, Mingyang Wei, Abdullah Y. Alsalloum, Partha Maity, Bekir Turedi, Chen Yang, Derya Baran, Thomas D. Anthopoulos, Yu Han, Zheng-Hong Lu, Omar F. Mohammed, Feng Gao, Edward H. Sargent, Osman M. Bakr, Managing grains and interfaces via ligand anchoring enables 22.3%-efficiency inverted perovskite solar cells, Nat. Energy 5 (2) (2020) 131–140.
[69] Jin-Wook Lee, Sang-Hoon Bae, Yao-Tsung Hsieh, Nicholas De Marco, Mingkui Wang, Pengyu Sun, Yang Yang, A Bifunctional Lewis Base Additive for Microscopic Homogeneity in Perovskite Solar Cells, Chem 3 (2) (2017) 290–302.
[70] L. Liang, H. Luo, J. Hu, H. Li, P. Gao, Efficient Perovskite Solar Cells by Reducing Interface-Mediated Recombination: a Bulky Amine Approach, Adv. Energy Mater. 10 (2020) 2000197–2000208.
[71] Shaobing Xiong, Zhangyu Hou, Shijie Zou, Xiaoshuang Lu, Jianming Yang, Tianyu Hao, Zihao Zhou, Jianhua Xu, Yihan Zeng, Wei Xiao, Wei Dong, Danqin Li, Xiang Wang, Zhigao Hu, Lin Sun, Yuning Wu, Xianjie Liu, Liming Ding, Zhenrong Sun, Mats Fahlman, Qinye Bao, Direct Ob servation on p-to n-Type Transformation of Perovskite Surface Region during Defect Passivation Driving High Photovoltaic Efficiency, Joule 5 (2) (2021) 467–480.
[72] Q. Cao, Y. Li, H. Zhang, J. Yang, J. Han, T. Xu, S. Wang, Z. Wang, B. Gao, J. Zhao, X. Li, X. Ma, S.M. Zakeeruddin, W.E.I. Sha, X. Li, M. Grätzel, Efficient and stable inverted perovskite solar cells with very high fill factors via incorporation of star-shaped polymer, Sci. Adv. 7 (2021) eabg0633.
[73] X. Yin, J. Zhou, Z. Song, Z. Dong, Q. Bao, N. Shrestha, S.S. Bista, R.J. Ellingson, Y. Yan, W. Tang, Dithieno[3,2-b:2′,3′-d]pyrro l-Cored Hole Transport Material Enabling Over 21% Efficiency Dopant-Free Perovskite Solar Cells, Adv. Funct. Mater. 29 (2019) 1904300–1904308.
[74] T. Li, S. Wang, J. Yang, X. Pu, B. Gao, Z. He, Q. Cao, J. Han, X. Li, Multiple functional groups synergistically improve the performance of inverted planar perovskite solar cells, Nano Energy 82 (2021) 105742–105751.
[75] N. Li, X. Niu, Q. Chen, H. Zhou, Towards commercialization: the operational stability of perovskite solar cells, Chem. Soc. Rev. 49 (2020) 8235–8286.